

# Designing Low-Carbon, Low-Temperature Bainite

Hong-Seok Yang and H. K. D. H. Bhadeshia

Graduate Institute of Ferrous Technology  
POSTECH, Hyoja-dong san 31, Pohang 790-784  
Republic of Korea  
<http://cml.postech.ac.kr>

## Abstract

The possibility of producing bainite at low temperatures by suppressing transformation using substitutional solutes has been investigated, as an alternative to using large carbon concentrations to achieve the same purpose. It is found that although transformation temperatures can indeed be suppressed in this way, the difference between the bainite and martensite-start temperatures diminishes. This, combined with the relatively low carbon concentration of the steels studied, promotes the coarsening of the microstructure via a coalescence of fine bainite plates, which may have detrimental consequences on the properties although this remains to be demonstrated. The study also reveals the need for a better interpretation of the bainite-start temperature to cover circumstances where the transformation times are unusually long.

## 1 Introduction

The scale and extent of the microstructure obtained when austenite transforms into bainite is dependent directly on the fact that the atoms move in a disciplined fashion. This information has been exploited to develop unconventional alloys based on carbide-free mixtures of bainitic ferrite and carbon-enriched retained austenite. Examples include the austempered ductile cast irons (1–3), TRIP-assisted steels (4–6), rail steels which do not rely on carbides for their properties (7; 8), and recently, the hardest ever bainite (9–14).

The hard bainite is particularly fascinating in that it can be produced in bulk form, without the need for rapid heat treatment or mechanical processing, by transformation at low temperatures (typically 200°C), resulting in plates of ferrite which are remarkably thin (20–40 nm). This fine scale of the microstructure is largely responsible for hardnesses as high as 690 HV (11; 13). The very low transformation temperature is achieved primarily by increasing the carbon concentration of the steel to about 1 wt% (15). This might make the alloys difficult to weld because of the danger of forming untempered, brittle martensite in the heat-affected zones of any joints. Coarse martensite is prone to fracture under the influence of small stresses (16), in which case it would compromise the structural integrity of the joint. For this reason, the vast majority of weldable steels have low carbon concentrations.

Since much of the strength of the bainite comes from its fine scale and not from dissolved carbon, it should be possible to reduce its concentration and instead to suppress the transformation temperature using substitutional solutes. One obvious requirement is that the bainite-start temperature ( $B_S$ ) must be maintained above that for martensite ( $M_S$ ).

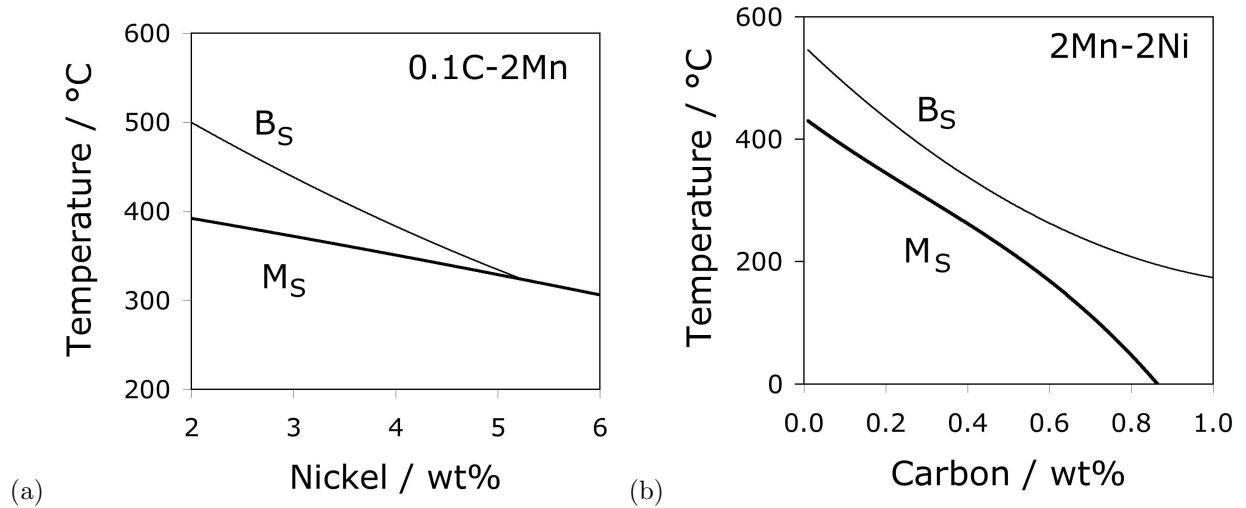


Figure 1: Calculated bainite and martensite–start temperatures (21): (a) Fe–0.1C–2Mn wt%, with a variation in nickel concentration; (b) Fe–2Ni–2Mn with a variation in the carbon concentration.

Published calculations done using theory described elsewhere (17–20) indicate that carbon is much more effective at maintaining a difference between the  $M_S$  and  $B_S$  temperatures than are substitutional solutes, Fig. 1 (21). Substitutional atoms do not partition at any stage in the formation of martensite or bainite. Carbon, however, does so during the nucleation stage of bainite, making the latter different from martensite which nucleates and grows without diffusion (Table 1). As a consequence bainite can form at a higher temperature than martensite. This advantage is diminished if carbon concentration is reduced, as illustrated in Figure 1b.

The results presented in Fig. 1 are discouraging from the perspective of designing a low-carbon bainite with a fine microstructure obtained by transforming at low temperatures. However, the issue is worth investigating further since the original theory has a number of approximations to be discussed later. The purpose of the present work was to explore the Fe–Mn–Ni–C system in the context of these calculations, bearing in mind the desire to design low-carbon alloys in which the  $B_S$  temperature is suppressed.

Table 1: The mechanisms of displacive transformations used in the quantitative expression of phases (17; 20; 22). ‘Paraequilibrium’ implies the partitioning of carbon between the parent and product phases, subject to the constraint that the ratio of substitutional solute to iron atoms is maintained constant (23–29).

	Martensite $\alpha'$	Bainite $\alpha_b$	Widmanstätten ferrite $\alpha_W$
Nucleation	Diffusionless	Paraequilibrium	Paraequilibrium
Growth	Diffusionless	Diffusionless	Paraequilibrium

## 2 Experimental Method

A technique usually applied to manufacture standards for chemical analysis was used to make the alloys. Solid cylindrical-samples of dimensions  $3.6 \times 8$  cm were centrifugally cast and then homogenised in a vacuum furnace for two days at 1200 °C. The length of each sample was then cut into five or six pieces of equal

thickness; their individual chemical analyses are shown in Table 2. The carbon concentration was analysed using a LECO instrument to a reproducibility of  $\pm 0.0013$  wt%, and the remaining elements using spark optical emission spectroscopy to a reproducibility of  $\pm 0.003$  wt%. These chemical composition data can be used to estimate the expected variation in the martensite–start temperature. Using the methodology described elsewhere (18; 19), the variation expected on the basis of the tabulated compositions is estimated to be less than  $\pm 2^\circ\text{C}$ .

Table 2: Chemical compositions in wt%

Designation	4Ni			5Ni			6Ni		
Sample	Mn	Ni	C	Mn	Ni	C	Mn	Ni	C
1	2.28	4.04	0.132	2.26	5.02	0.124	2.51	6.72	0.203
2	2.28	4.04	0.132	2.28	5.03	0.126	2.51	6.74	0.203
3	2.28	4.03	0.130	2.26	5.01	0.126	2.48	6.71	0.201
4	2.25	4.02	0.132	2.28	5.05	0.126	2.51	6.77	0.201
5	2.28	4.03	0.130	2.24	4.97	0.123	2.51	6.75	0.202
6	2.28	4.04	0.132	2.28	5.04	0.127			
Average	2.275	4.033	0.1313	2.27	5.02	0.125	2.50	6.74	0.202

Cylindrical dilatometric samples of diameter 4 mm and length 7 mm were machined, some of which were made hollow by drilling a 3 mm diameter longitudinal hole. As shown previously (30), the hollow samples gave identical results within experimental error to the solid samples.

A push–rod *BAHR DIL805* high–speed dilatometer was used, with radio frequency induction heating and a strain resolution of  $7.1 \times 10^{-6}$ , corresponding to a martensite volume fraction of  $1.1 \times 10^{-3}$ . The sample temperature is measured by a thermocouple welded to its surface using a precision welder and jig supplied by the dilatometer manufacturer. Each sample was austenitised in a vacuum ( $5 \times 10^{-4}$  mbar) at  $950^\circ\text{C}$  for the 4Ni and 5Ni samples and  $900$  or  $950^\circ\text{C}$  for the 6Ni samples. The 4Ni samples were austenitised for 3 minutes and the others for 5 minutes. Details of the martensite–start temperature measurements have been published elsewhere (30) but isothermal transformation experiments were carried out by quenching the sample to the set temperature using helium gas.

The interpretation of dilatometric data can be subjective especially in assessing the onset of transformation (30). To overcome these difficulties, a method has recently been proposed (30) in which the data are interpreted by defining the first onset of transformation to be that at which a critical strain  $\epsilon_C$  is achieved relative to the thermal contraction of the parent phase.  $\epsilon_C$  is calculated for 1 volume percent of martensitic transformation assuming that the latter occurs at room temperature, by using published equations for the lattice parameters of austenite and martensite (30). This ensures that the method is reproducible and emphasises that transformation–start temperatures should be quoted with the value of the critical strain used to interpret the dilatometric data. This is the method used throughout the present work.

Samples for transmission electron microscopy were prepared from  $300 \mu\text{m}$  thick slit–samples which were then reduced in thickness from both sides using SiC paper to a thickness of about  $80 \mu\text{m}$  before punching out 3 mm discs. These foils were electropolished at room temperature, until perforation occurred, using a *Tenupol-5* polisher set at 20–40 V. The electrolyte consisted of 6–8% perchloric acid and 92–94% acetic acid. The thin foils were examined in a *Philips CM200* transmission electron microscope operated at 200 kV.

Samples for optical microscopy were etched using a solution of 1 g sodium metabisulfite in 100 ml water

mixed with 4 g of picric acid dissolved in 100 ml of water, for 1–30 s.

### 3 Martensite–Start Temperatures

Typical dilatometric experiments are illustrated in Fig. 2 and measured values of the  $M_S$  temperatures, determined using the offset method (30) are presented in Table 3. The  $M_S$  data for the 4Ni alloy are from (30) where the method for assessing dilatometric data was developed. A large number of experiments were done in some cases in order to gain confidence in the technique but the measurements are reliable so four experiments were deemed to be sufficient in the case of the 5Ni alloy. Notice that the observed level of scatter is consistent with expectations (30).

Table 3: Measured  $M_S$  temperatures.

Alloy	$M_S/^{\circ}\text{C}$								Mean	Standard Deviation
4Ni	377	376	363	372	358	363	361	401	373	12
	392	366	372	370	385	375	365	–		
5Ni	361	360	383	382	–	–	–	–	372	13
6Ni	265	258	292	290	278	278	284	285	272	14
	253	252	260	264	270	–	–	–		

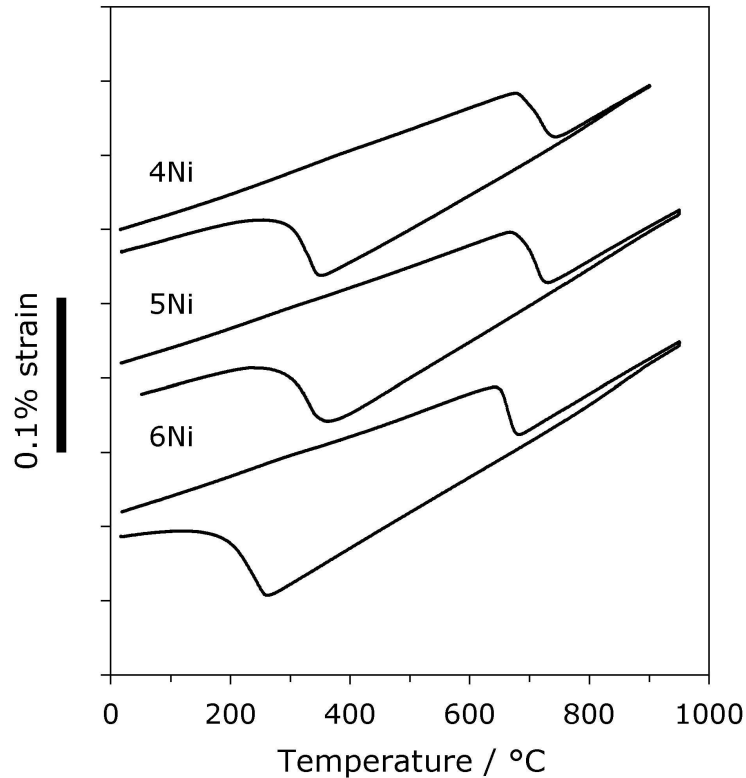


Figure 2: Typical dilatometric data for martensite–start temperature determinations.

## 4 Bainite

Dilatometric data from isothermal transformation experiments on the three alloys are illustrated in Fig. 3 along with hardness values measured on the samples following transformation. Bainite can only form below the  $T_0$  temperature where austenite and ferrite of the same chemical composition have identical free energies; the highest temperature at which it can form will in fact be lower, at  $T'_0$ , in order to account for strain energy and nucleation phenomena. This  $T'_0$  condition limits the maximum fraction of bainite to zero at  $B_S$  to values which increase with the undercooling below the start temperature. This is precisely what is observed in Figs. 3a–c. Samples of the 6Ni alloy showed very little reaction so one specimen was held for a prolonged period of 31 h at 280°C to establish that bainite can in fact form (Fig. 3c). The hardness data are consistent with the dilatometric experiments; in Fig. 3d the hardness values of quenched fully-martensitic samples are included for reference since the formation of bainite leads to a reduction in hardness, depending on the fraction of bainite.

It is noticeable in Fig. 3 that the maximum extent of transformation decreases towards zero as the temperature increases towards  $B_S$ . This is because of the incomplete reaction phenomenon in which diffusionless transformation can only occur if the composition of the residual austenite is below that corresponding to the  $T'_0$  curve on the phase diagram (31; 32). This phenomenon is widely reported and is extremely useful in the design of steels (33; 33–37).

Comprehensive metallographic experiments were conducted on all the specimens in order to verify the occurrence of bainite and martensite in the three alloys, including both optical and transmission electron microscopy; only a few of these observations are reported here for the sake of brevity but the complete set is available elsewhere for examination<sup>1</sup>.

Considering first the 4Ni alloy, Fig. 4 illustrates how bainite appears in an optical micrograph for the sample transformed isothermally at 440°C together with residual regions which were austenite at the transformation temperature but now are regions of martensite. As expected from the dilatometric and hardness data, transformation at 490°C failed to produce bainite so it can be concluded that  $480^\circ\text{C} < B_S < 490^\circ\text{C}$  since bainite was observed on transformation at 480°C. A transmission electron micrograph of the bainite is also shown, illustrating the typical thin-platelets separated by residual carbon-enriched austenite which decomposes in this alloy to martensite on cooling. Retained austenite could not be detected using X-ray diffraction as illustrated in Fig. 5. On the basis of these experiments, the  $B_S$  temperature of Alloy 4Ni is taken to be  $485 \pm 10^\circ\text{C}$ , where the stated uncertainty is probably twice as large as the experiments might indicate, to allow for greater statistical confidence in the interpretation of the data.

The bainite-start temperature for alloy 5Ni was similarly established to be  $465 \pm 10^\circ\text{C}$ ; typical microstructures are illustrated in Fig. 6, and it is emphasised again that all the transformed samples were studied metallographically and found to be consistent with this interpretation of the start-temperature.

There is greater uncertainty for alloy 6Ni because of the very slow transformation rate but from the dilatometric data  $B_S$  is likely to be less than  $300^\circ\text{C}$  and has been assumed to be  $300 \pm 15^\circ\text{C}$ . The prolonged dilatometric experiment at  $280^\circ\text{C}$  was to check for the formation of bainite at a significant undercooling, but it is not practical to use such instruments for really long heat treatments. Therefore, another experiment was conducted by transforming a sealed sample in a furnace at  $280^\circ\text{C}$  for 12 weeks in order to study the resulting bainite. Fig. 7 shows the nature of bainite following this long heat treatment. The bainite regions obtained by transformation at  $280^\circ\text{C}$  seem blocky when examined using optical microscopy and although the transmission electron microscopy reveals the platelets (Fig. 7b) they are in blocky formations. This is quite unlike the thin, long and slender well-defined plates typical of the high-carbon low-temperature bainitic steels (15).

---

<sup>1</sup><http://cml.postech.ac.kr/2007/Ni/Ni.html>

The clue to the development of morphology comes from Fig. 8 where it is seen that there is a coalescence process at play in which fine platelets merge at their trailing edges to form coarser blocks. The fine platelets are of the order of 20 nm thick but the coalesced regions (marked ‘A’ and ‘B’) are much coarser. This coalescence of bainite platelets has previously been reported in steels (38; 39) and more recently in weld metals (40–42); the subject has been reviewed (43). The mechanism may be summarised as follows.

Coalesced bainite begins as a series of adjacent, identically oriented platelets of ferrite only marginally separated by films of austenite. As the platelets lengthen, they accelerate and coalesce. Electron back scattered diffraction has confirmed that the coalescence leads to a crystallographically homogeneous grain although small misorientations can be detected across the large plates due to plastic accommodation effects (44). The carbon is then trapped in the ferrite, either to precipitate later or to partly partition into the residual austenite at the peripheries of the cluster of platelets. Because the coalescence cannot involve diffusion, it can only occur when the driving force available is sufficient to sustain the greater strain energy associated with the coarser plates.

Of relevance here is the relatively low carbon concentration and the reduced transformation temperature which permits the individual platelets to develop without intervening films of austenite, leading to the coalescence process. Although not proven here, the coalescence process works against the development of a fine microstructure and hence may be a limiting factor in the design of steels in which substitutional solutes are utilised to suppress the transformation temperature. The low temperature is needed to obtain a fine microstructure (45–48).

## 5 Analysis of the Transformation Temperatures

All calculations presented here exploit MTDATA (49) combined with the SGTE database to evaluate the free energies of the phases, using an algorithm (50) based on the rationalisation of transformations in steels (17).

Both bainite and martensite must form below the  $T'_0$  temperature and this is indeed found to be the case as illustrated in Fig. 9. Consistent with the predictions in Fig. 1b, the difference between the  $B_S$  and  $M_S$  temperatures decreases as the nickel concentration increases, becoming only 30°C for alloy 6Ni. It is interesting that this is one of the conditions for the onset of coalesced bainite (51).

There are two equations which have to be simultaneously satisfied before bainite formation becomes possible at  $B_S$  (17; 22; 52). The first corresponds to a growth criterion that there must be sufficient free energy available to sustain diffusionless transformation together with a strain energy of some 400 J mol<sup>-1</sup>. The second is a nucleation condition in which the free energy change calculated allowing for carbon partitioning between the parent and product phases must exceed a value given by a nucleation function. Either one of these conditions can become redundant depending on circumstances.

If the nucleation condition is redundant then  $B_S = T'_0$ , which appears to be the case for alloys 4Ni and 5Ni as shown in Fig. 9. However, the nucleation condition becomes controlling when the transformation is suppressed by alloying because of the reduced thermal activation. It is reasonable therefore for the measured  $B_S$  to be closer to the nucleation limited  $B_S$  for alloy 6Ni and well below  $T'_0$ . The measured  $B_S$  should not of course be above that calculated, as is the case for alloy 6Ni, but the reason for this is the exceptionally high transformation time used, which is not catered for by the original derivation of the nucleation function. The original work utilised a detectable nucleation rate at the highest transformation temperature (equations 2–3 (17)), fitted empirically to ordinary steels listed in an atlas of isothermal transformation diagrams. Naturally, if a much lower detectable nucleation rate is defined by using an excessively large transformation time then the calculated  $B_S$  would increase to any point below the  $T'_0$  temperature. There clearly is a need to improve

interpretation in order to deal with very slow transforming steels which have now assumed technological significance (53). In essence, for steels in which  $B_S < T'_0$ , it should be possible by using long heat treatments to eventually obtain bainite. If there is no limit placed on the heat-treatment time then the bainite-start temperature must be given by  $T'_0$  assuming that other transformations which normally are kinetically disadvantaged relative to bainite, do not intervene.

Finally, it is worth emphasising that with Alloy 6Ni which is nucleation limited,  $B_S \ll T'_0$  which means that there is excess free energy available to sustain the greater strain energy associated with the coalescence process. This is not the case with Alloys 4Ni and 5Ni where coalescence is not observed.

## 6 Summary

In previous work, it has been shown that incredibly fine bainitic microstructures can be produced in bulk steel by suppressing the bainite transformation temperature, primarily by alloying with about 1 wt% carbon. The aim in the present work was to use substitutional solutes to achieve the same purpose while keeping the carbon concentration small.

It is found that the bainite-start temperature can indeed be suppressed in this way, but unlike the high-carbon steels, the difference between  $B_S$  and  $M_S$  decreases dramatically at high solute concentrations, as predicted theoretically. Furthermore,  $B_S \ll T'_0$  so that there is excess free energy available during the course of transformation. Consequently, the fine platelets of bainite that are initiated tend to coalesce during the growth stage, perhaps negating the advantage of transforming at low temperatures. The consequences of the coalescence on properties requires further investigation. The work has also highlighted the need for improved interpretation of transformation-start temperatures in order to cope with very slow reaction at low homologous temperatures.

## 7 Acknowledgements

We are grateful to Professor Hae-Geon Lee for the provision of laboratory facilities at GIFT, POSTECH, to Professor Sung-Mo Jung for the manufacture of the alloys and to Professor Bruno de Cooman for access to a precision dilatometer.

## References

- [1] E. Dorazil, B. Barta, E. Munsterova, L. Stransky, and A. Huvar. High strength bainitic ductile cast iron. *AFS International Cast Metals Journal*, 22:52–62, 1982.
- [2] D. J. Moore, T. N. Rouns, and K. B. Rundman. Structure and mechanical properties of austempered ductile iron. *AFS Transactions*, 93:705–718, 1985.
- [3] O. Matsumura, Y. Sakuma, and H. Takechi. TRIP and its kinetic aspects in austempered 0.4C-1.5Si-0.8Mn steel. *Scripta Metallurgica*, 27:1301–1306, 1987.
- [4] E. Girault. *Bainitic transformation in TRIP-assisted steels and its influence on mechanical properties*. PhD thesis, Katholieke Universiteit Leuven, Belgium, 1999.

- [5] P. J. Jacques. Transformation-induced plasticity for high strength formable steels. *Current Opinion in Solid State and Materials Science*, 8:259–265, 2004.
- [6] B.C. DeCooman. Structure–properties relationship in TRIP steels containing carbide-free bainite. *Current Opinion in Solid State and Materials Science*, 8:285–303, 2004.
- [7] H. K. D. H. Bhadeshia. Steels for rails. In *Encyclopedia of Materials Science*, pages 1–7. Pergamon Press, Oxford, Elsevier Science, 2007.
- [8] M. R. Zhang and H. C. Gu. Microstructure and properties of carbide free bainite railway wheels produced by programmed quenching. *Materials Science and Technology*, 23:970–974, 2007.
- [9] F. G. Caballero, H. K. D. H. Bhadeshia, K. J. A. Mawella, D. G. Jones, and P. Brown. Very strong, low-temperature bainite. *Materials Science and Technology*, 18:279–284, 2002.
- [10] C. Garcia-Mateo, F. G. Caballero, and H. K. D. H. Bhadeshia. Low-temperature bainite. *Journal de Physique Colloque*, 112:285–288, 2003.
- [11] C. Garcia-Mateo, F. G. Caballero, and H. K. D. H. Bhadeshia. Development of hard bainite. *ISIJ International*, 43:1238–1243, 2003.
- [12] C. Garcia-Mateo, F. G. Caballero, and H. K. D. H. Bhadeshia. Acceleration of low-temperature bainite. *ISIJ International*, 43:1821–1825, 2003.
- [13] M. Peet, C. Garcia-Mateo, F. G. Caballero, and H. K. D. H. Bhadeshia. Tempering of a hard mixture of bainitic ferrite and austenite. *Materials Science and Technology*, 20:814–818, 2004.
- [14] M. Peet, S. S. Babu, M. K. Miller, and H. K. D. H. Bhadeshia. Three-dimensional atom probe analysis of carbon distribution in low-temperature bainite. *Scripta Materialia*, 50:1277–1281, 2004.
- [15] F. G. Caballero and H. K. D. H. Bhadeshia. Very strong bainite. *Current Opinion in Solid State and Materials Science*, 8:186–193, 2005.
- [16] S. Chatterjee and H. K. D. H. Bhadeshia. TRIP-assisted steels: cracking of high carbon martensite. *Materials Science and Technology*, 22:645–649, 2006.
- [17] H. K. D. H. Bhadeshia. Rationalisation of shear transformations in steels. *Acta Metallurgica*, 29:1117–1130, 1981.
- [18] H. K. D. H. Bhadeshia. The driving force for martensitic transformation in steels. *Metal Science*, 15:175–177, 1981.
- [19] H. K. D. H. Bhadeshia. Thermodynamic extrapolation and the martensite-start temperature of substitutionally alloyed steels. *Metal Science*, 15:178–150, 1981.
- [20] H. K. D. H. Bhadeshia. *Bainite in Steels, 2nd edition*. Institute of Materials, London, 2001.
- [21] H. K. D. H. Bhadeshia. Hard bainite. In J. M. Howe, D. E. Laughlin, J. K. Lee, U. Dahmen, and W. A. Soffa, editors, *Solid-Solid Phase Transformations, TME-AIME, Warrendale, USA*, volume 1, pages 469–484, 2005.
- [22] H. K. D. H. Bhadeshia and J. W. Christian. The bainite transformation in steels. *Metallurgical & Materials Transactions A*, 21A:767–797, 1990.
- [23] A. Hultgren. Isothermal transformation of austenite. *Transactions of the American Society for Metals*, 39:915–1005, 1947.
- [24] A. Hultgren. Isotherm omvandling av austenit. *Jernkontorets Annaler*, 135:403–494, 1951.
- [25] M. Hillert. Användning av isoaktiva linjer i ternära tillstånd-diagram. *Jernkontorets Annaler*, 136:25–37, 1952.



- [26] H. I. Aaronson, H. A. Domian, and G. M. Pound. Thermodynamics of the austenite - poreutectoid ferrite transformation II, Fe-C-X alloys. *TMS-AIME*, 236:768–780, 1966.
- [27] H. I. Aaronson, H. A. Domian, and G. M. Pound. Partitioning of alloying elements between austenite and proeutectoid ferrite and bainite. *TMS-AIME*, 236:781–796, 1966.
- [28] H. K. D. H. Bhadeshia. Diffusional formation of ferrite in iron and its alloys. *Progress in Materials Science*, 29:321–386, 1985.
- [29] D. V. Malakhov and G. R. Purdy. Some fundamental and computational aspects of paraequilibrium. *Canadian Metallurgical Quarterly*, 41:231–242, 2002.
- [30] H.-S. Yang and H. K. D. H. Bhadeshia. Uncertainties in the dilatometric determination of the martensite-start temperature. *Materials Science and Technology*, 23:556–560, 2007.
- [31] H. K. D. H. Bhadeshia and D. V. Edmonds. The mechanism of bainite formation in steels. *Acta Metallurgica*, 28:1265–1273, 1980.
- [32] H. K. D. H. Bhadeshia and A. R. Waugh. Bainite: An atom probe study of the incomplete reaction phenomenon. *Acta Metallurgica*, 30:775–784, 1982.
- [33] H. K. D. H. Bhadeshia and D. V. Edmonds. Bainite in silicon steels: a new composition property approach i. *Metal Science*, 17:411–419, 1983.
- [34] M. Sherif, C. Garcia-Mateo, T. Sourmail, and H. K. D. H. Bhadeshia. Stability of retained austenite in TRIP-assisted steels. *Materials Science and Technology*, 20:319–322, 2004.
- [35] S. Chatterjee, H. S. Wang, J. R. Yang, and H. K. D. H. Bhadeshia. Mechanical stabilisation of austenite. *Materials Science and Technology*, 22:641–644, 2006.
- [36] S. Chatterjee, M. Murugananth, and H. K. D. H. Bhadeshia.  $\delta$ -TRIP steel. *Materials Science and Technology*, 23:819–827, 2007.
- [37] F. G. Caballero, H. K. D. H. Bhadeshia, K. J. A. Mawella, D. G. Jones, and P. Brown. Design of novel high-strength bainitic steels: Part i. *Materials Science and Technology*, 17:512–516, 2001.
- [38] H. K. D. H. Bhadeshia and D. V. Edmonds. The bainite transformation in a silicon steel. *Metallurgical Transactions A*, 10A:895–907, 1979.
- [39] L. C. Chang and H. K. D. H. Bhadeshia. Microstructure of lower bainite formed at large undercoolings below the bainite start temperature. *Materials Science and Technology*, 12:233–236, 1996.
- [40] E. Keehan, L. Karlsson, and H.-O. Andrén. Influence of C, Mn and Ni on strong steel weld metals: Part 1, effect of nickel. *Science and Technology of Welding and Joining*, 11:1–8, 2006.
- [41] E. Keehan, L. Karlsson, H.-O. Andrén, and H. K. D. H. Bhadeshia. Influence of C, Mn and Ni on strong steel weld metals: Part 2, increased impact toughness. *Science and Technology of Welding and Joining*, 11:9–18, 2006.
- [42] E. Keehan, L. Karlsson, H.-O. Andrén, and H. K. D. H. Bhadeshia. Influence of C, Mn and Ni on strong steel weld metals: Part 3, increased strength. *Science and Technology of Welding and Joining*, 11:19–24., 2006.
- [43] H. K. D. H. Bhadeshia. Coalesced bainite. *Transactions of the Indian Institute of Metals*, 59:689–694, 2006.
- [44] H. K. D. H. Bhadeshia E. Keehan, L. Karlsson and M. Thuvander. An electron backscattering diffraction study of coalesced bainite in high-strength steel weld metals. *Materials Science and Technology*, 23:in press., 2007.

- [45] S. B. Singh and H. K. D. H. Bhadeshia. Estimation of bainite plate-thickness in low-alloy steels. *Materials Science and Engineering A*, A245:72–79, 1998.
- [46] K. J. Irvine and F. B. Pickering. High carbon bainitic steels. In *Physical properties of martensite and bainite, special report 93*, pages 110–125, London, 1965. Iron and Steel Institute.
- [47] M. J. Hawkins and J. Barford. Experimental kinetics of bainite formation. *Journal of the Iron and Steel Institute*, 210:97–105, 1972.
- [48] G. Ghosh and V. Raghavan. Kinetics of isothermal martensitic transformation in an Fe–23.2Ni–2.8Mn alloy. *Materials Science and Engineering*, 80:65–74, 1986.
- [49] NPL. MTDATA. Software, National Physical Laboratory, Teddington, U.K., 2006.
- [50] T. Okumura. MAP\_STEEL\_MTTTDDATA,  
<http://www.msm.cam.ac.uk/map/steel/programs/MTTTDDATA.html>.
- [51] H.-O. Andrén E. Keehan, L. Karlsson and L-E. Svensson. New developments with C–Mn–Ni high strength steel weld metals: Properties. *Welding Journal, Research Supplement*, 85:211s–218s, 2006.
- [52] H. K. D. H. Bhadeshia. A thermodynamic analysis of isothermal transformation diagrams. *Metal Science*, 16:159–165, 1982.
- [53] H. K. D. H. Bhadeshia. Large chunks of very strong steel. *Materials Science and Technology*, 21:1293–1302, 2005.

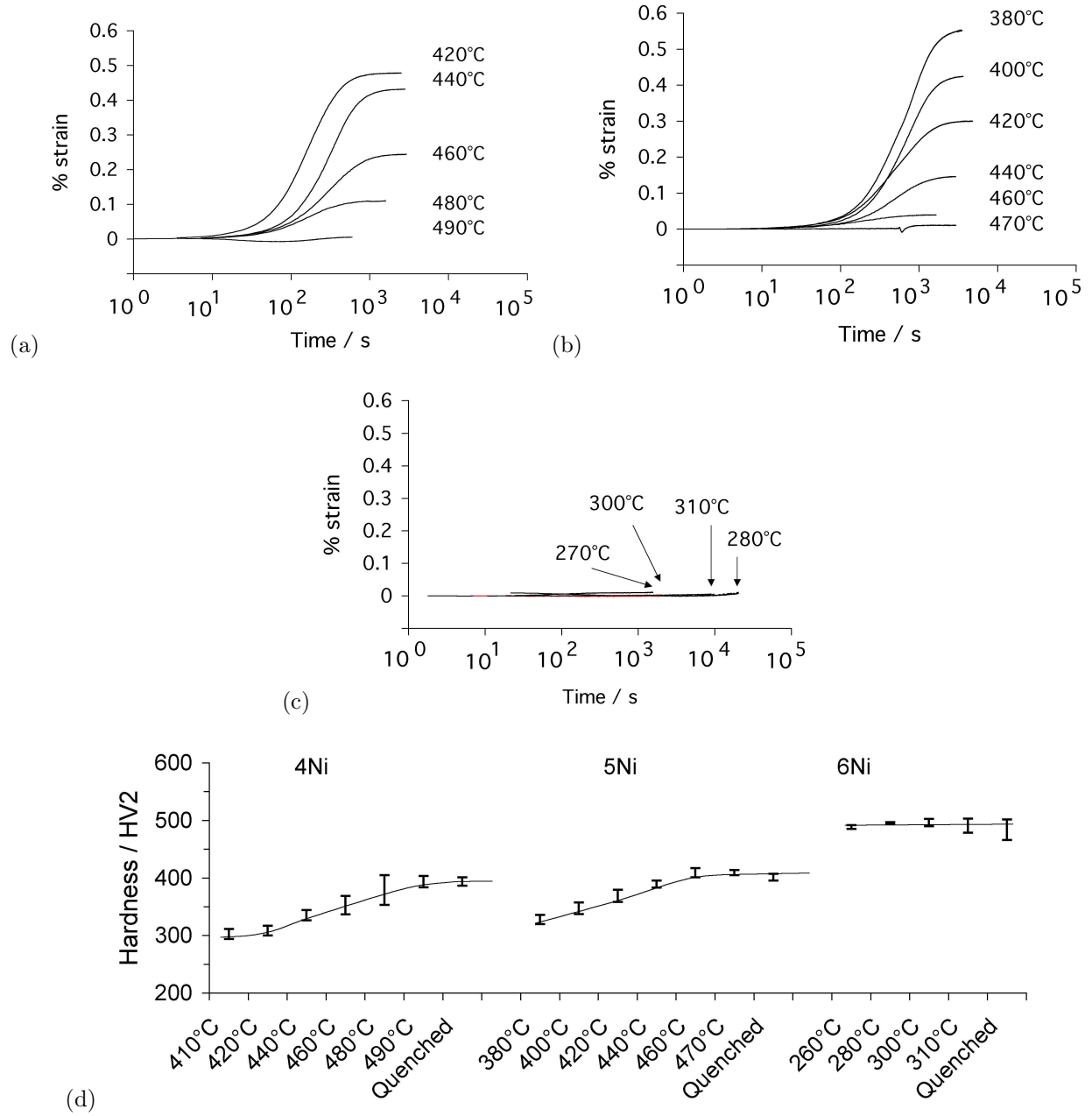


Figure 3: Isothermal transformation dilatometric curves exploring the formation of bainite. (a) Alloy 4Ni, (b) Alloy 5Ni, (c) Alloy 6Ni – in this figure, the end points of the experiments are marked for clarity. (d) Vickers hardness data measured using a 2 kg load. The temperatures correspond to isothermal transformation experiments.

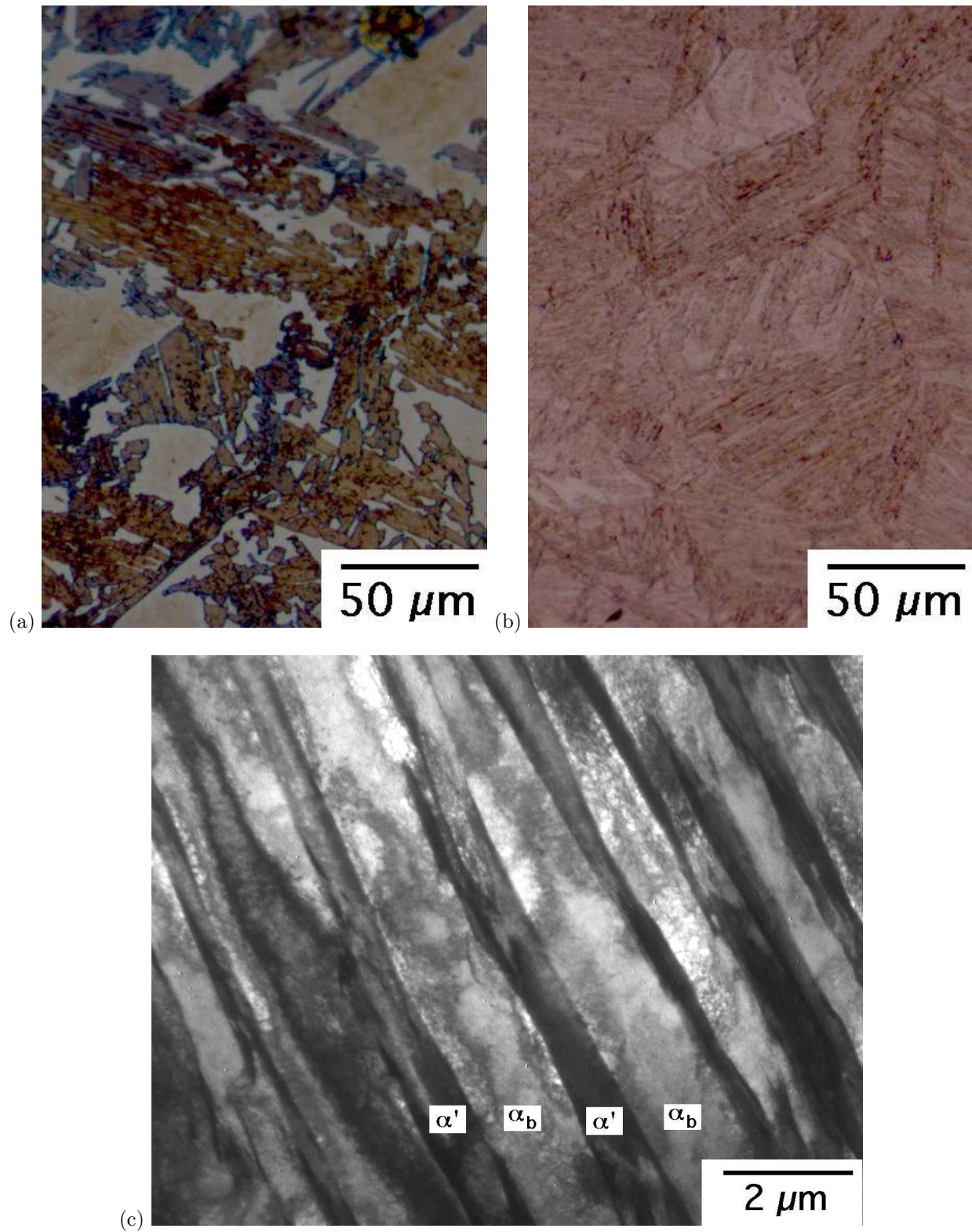


Figure 4: Sample 4Ni. Colour optical micrographs, (a) transformed isothermally at 440°C – the light brown regions are martensitic, (b) transformed isothermally at 490°C showing fully martensitic microstructure. (c) Transmission electron micrograph from sample transformed isothermally at 460°C, showing a mixture of bainitic ferrite platelets separated by regions of martensite.

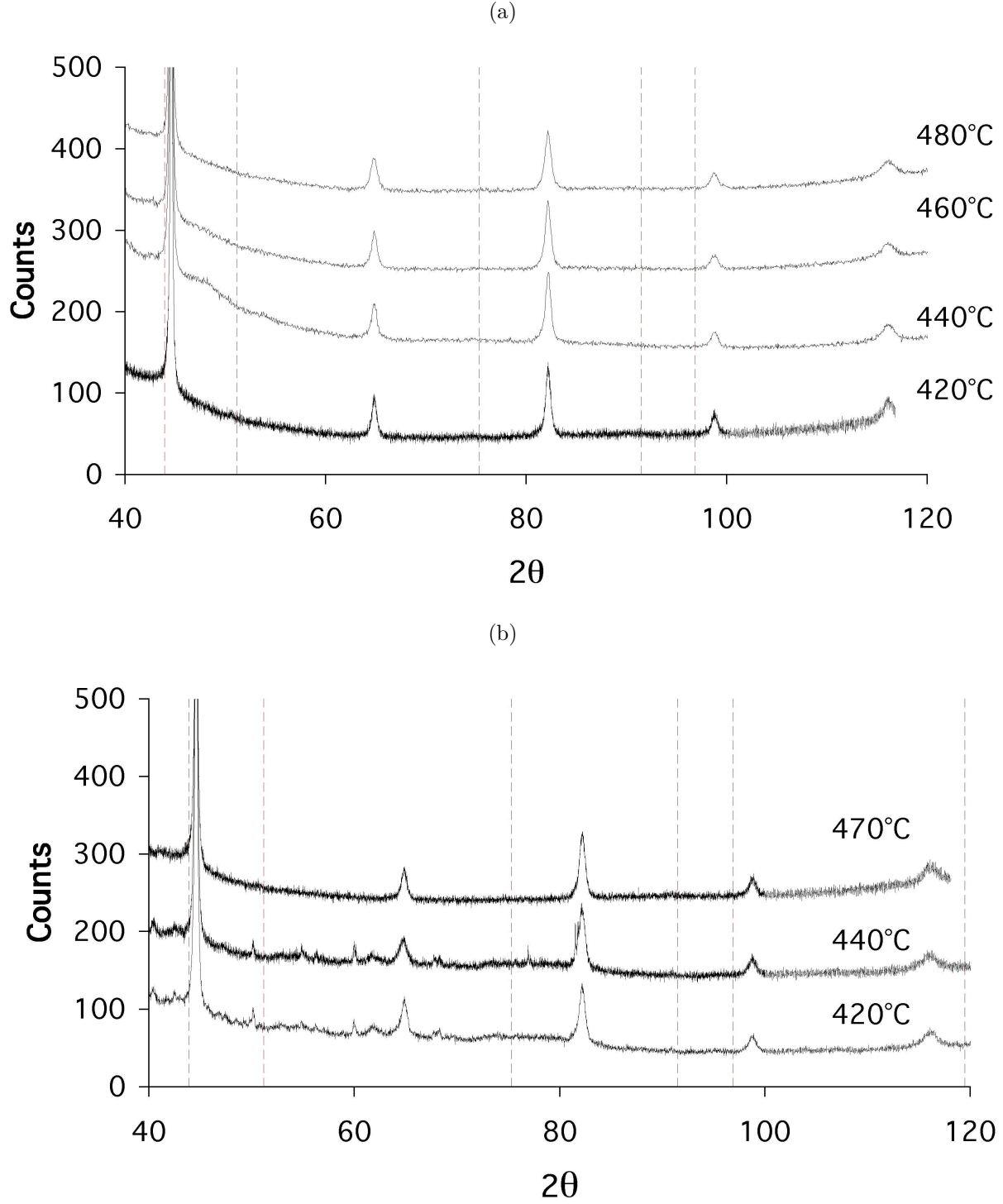


Figure 5: X-ray diffraction patterns taken using  $\text{CuK}\alpha$  radiation. The ferrite peaks, in ascending order of  $2\theta$  can be indexed as 110, 002, 121, 022, 031 and 222 respectively. The positions of possible austenite peaks are marked as lines, and in ascending order of  $2\theta$  are 111, 200, 220, 112, 222, and 004 respectively. Transformation temperatures are also indicated. (a) Sample 4Ni, (b) sample 5Ni.



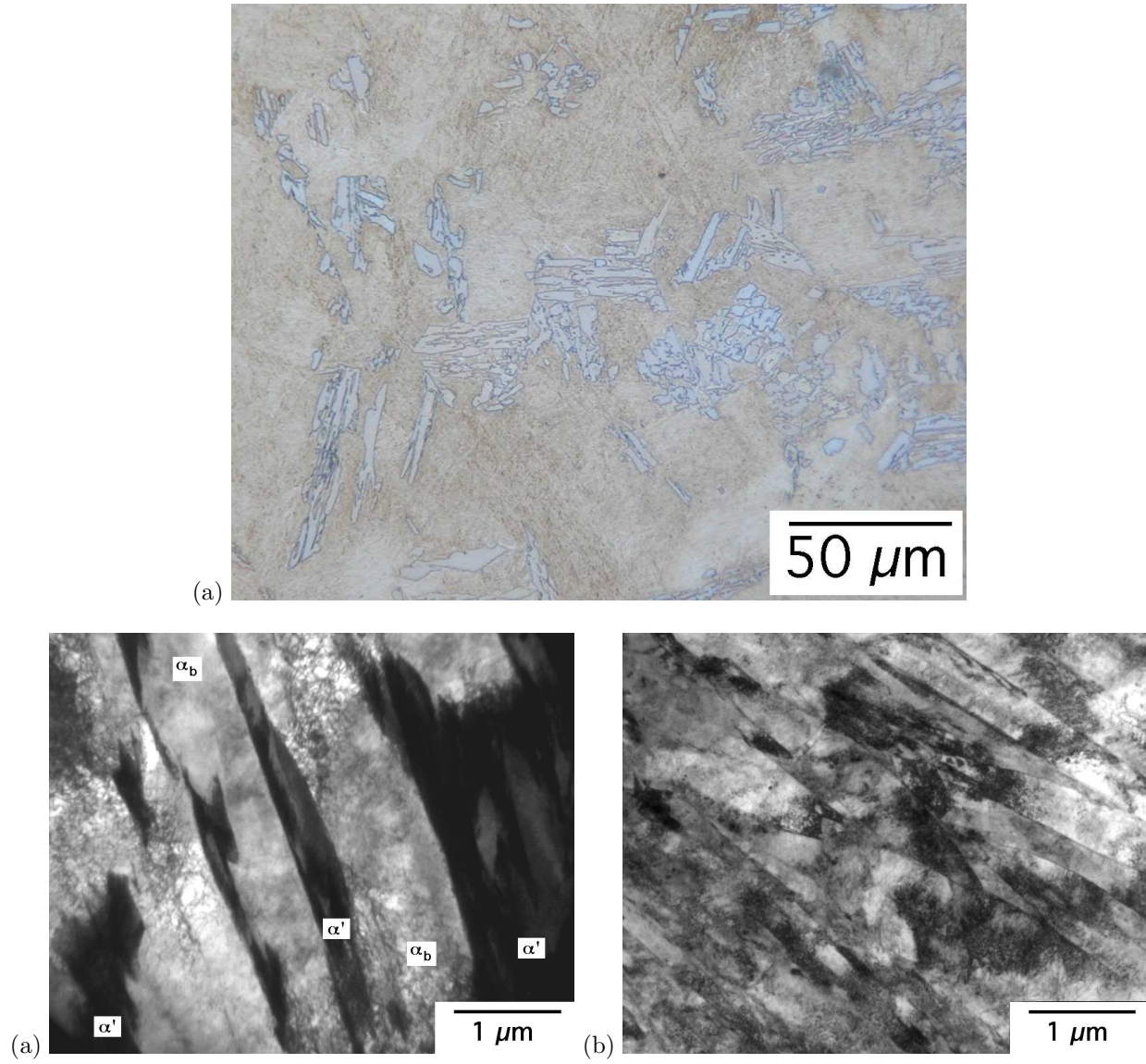


Figure 6: Sample 5Ni transformed isothermally at 440°C. (a) Optical micrograph showing a limited amount of bainite in a martensitic matrix. (b) Transmission electron micrograph showing a mixture of bainitic ferrite platelets with residual martensite. (b) Another region which is fully martensitic.

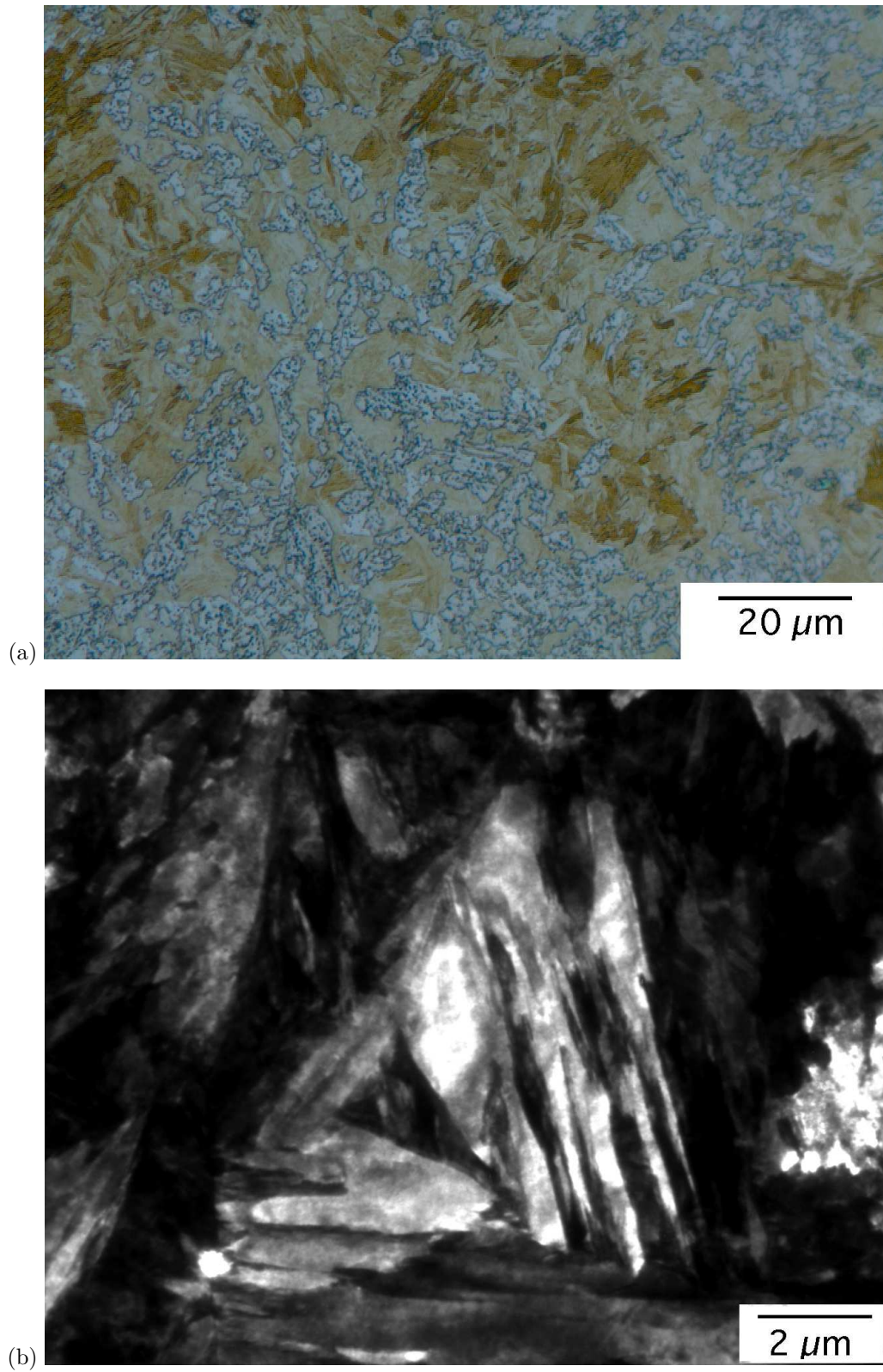


Figure 7: Sample 6Ni, transformed isothermally at 280°C for 12 weeks. (a) Optical micrograph, (b) transmission electron micrograph.

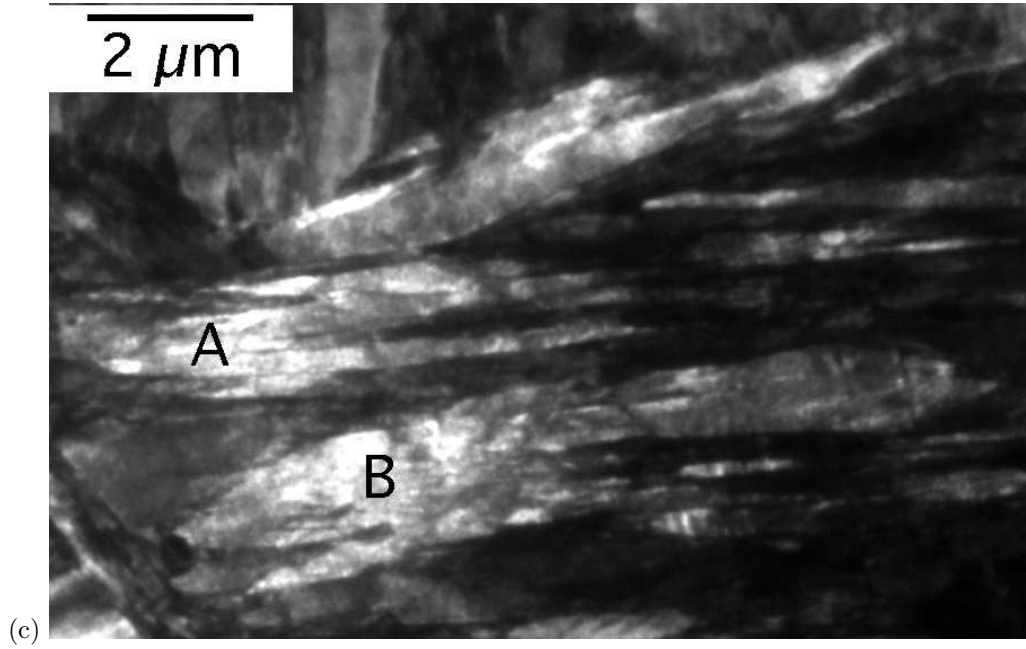


Figure 8: Sample 6Ni, transformed isothermally at 280°C for 12 weeks (c) transmission electron micrograph. The annotations ‘A’ and ‘B’ mark regions where coalescence has occurred – the participating platelets are towards the right of each coalesced region.

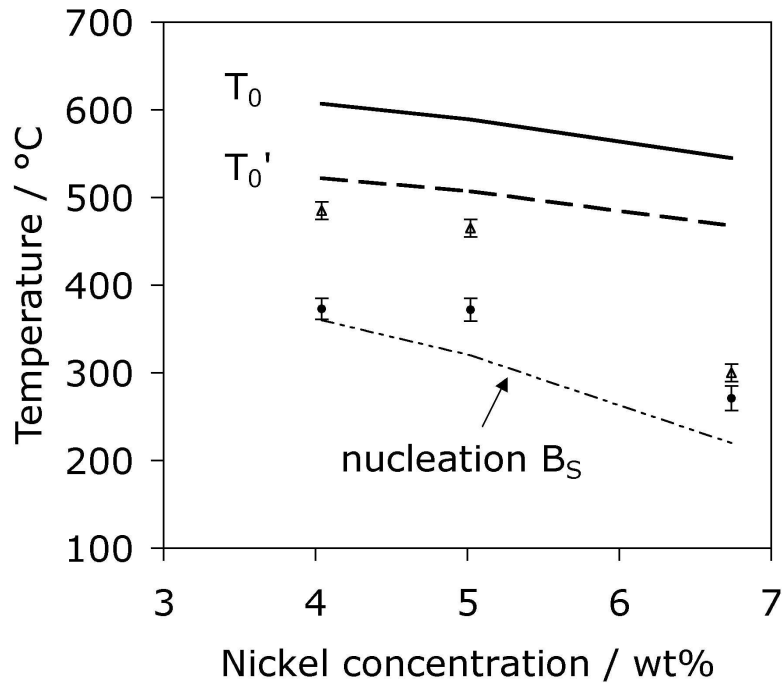


Figure 9: Calculated  $T_0$  and  $T'_0$  curves and measured martensite-start (circles) and bainite-start temperatures (triangles). The calculated nucleation-limited  $B_S$  is also illustrated.